NANO LETTERS

pubs.acs.org/NanoLett Letter

Terahertz Metagrating Emitters with Beam Steering and Full Linear Polarization Control

Cormac McDonnell,[+] Junhong Deng,[+] Symeon Sideris, Guixin Li,* and Tal Ellenbogen*

Cite This: https://doi.org/10.1021/acs.nanolett.1c04135 Read Online

ACCESS | Metrics & More | Article Recommendations | Supporting Information

ABSTRACT: We report the realization of broadband THz plasmonic metagrating emitters for simultaneous beam steering and all-optical linear polarization control. Two types of metagratings are designed and experimentally demonstrated. First, the plasmonic meta-atoms are arranged in a metagrating with a binary phase modulation which results in the nonlinear generation of THz waves to the ±1 diffraction orders, with complete suppression of the zeroth order. Complete tunability of the diffracted THz linear polarization direction is demonstrated through simple rotation of the pump polarization. Then, the concept of lateral phase shift is introduced into the design of the metagratings using interlaced phase gradients. By controlling the spatial shift of the submetagrating, we are able to continuously control the linear polarization states of the generated THz waves. This method results in a higher nonlinear diffraction efficiency relative to binary phase modulation. These functional THz metagratings show exciting promise to meet the challenges associated with the current diverse array of applications utilizing THz technology.

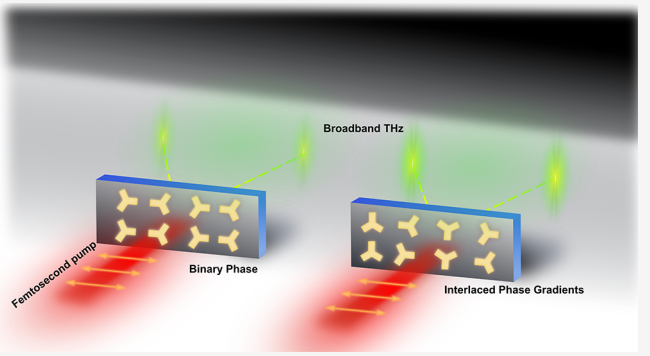

KEYWORDS: *Nonlinear metasurface, Terahertz (THz), Beam steering, Polarization control, Pancharatnam−Berry phase*

The terahertz (THz) region of the electromagnetic spectrum has gained widespread attention in a growing number of practical applications including biomedical imaging and spectroscopy,[1−3] nondestructive testing,[4,5] security,[6,7] and next generation wireless communications.[8,9] In addition, it is becoming increasingly useful for a variety of fundamental studies, e.g., monitoring crystal growth,[10] studies of topological insulators,[11] molecular rotations in the gas phase,[12] and manipulation of spin waves.[13] In order to optimize and fully exploit these emerging applications, full control over the THz waveform is required. In particular, the ability to steer the THz waves and maintain control over their polarization is instrumental to most of the applications mentioned above. Therefore, over the years, various methods have been developed to answer this need.

For beam steering, various types of grating devices have been developed specifically for the THz frequency band.[14−17] Similarly, for polarization control, passive elements, such as wire grid polarizers[18] and waveplates,[19] or active elements, such as spintronic heterostructures[20−22] and recently free space Kirigami polarization modulators,[23] have been demonstrated. Furthermore, fast modulation of the linear polarization direction of THz waves has also been shown using spintronic emitters at rates of up to 10 kHz.[24] This polarization switching may have important applications in polarization modulation spectroscopy.[25,26]

Almost all of these elements provide post control of the emission properties of THz sources such as quantum cascade lasers, nonlinear crystals, or photoconductive antennas.[27] However, such free space manipulation of THz waves usually requires additional optical elements and encounters significant limitations related mainly to absorption, width of manipulation bandwidth, and lack of good detectors. Therefore, it is important to develop new methodologies for functional THz wave manipulation that are free of the above limitations. One emerging direction involves the development of active nonlinear THz metasurface emitters.

In recent years, nonlinear metasurfaces have become a promising platform for the generation and control of electromagnetic radiation at optical frequencies. These metasurfaces consist of a thin layer of nanostructured metallic or high-index dielectric meta-atoms that exhibit nonlinear optical properties and can be used for generation of light at new frequencies. A wide variety of demonstrations of frequency conversion by nonlinear metasurfaces have been

Received: October 26, 2021
Revised: March 10, 2022

https://doi.org/10.1021/acs.nanolett.1c04135
Nano Lett. XXXX, XXX, XXX−XXX

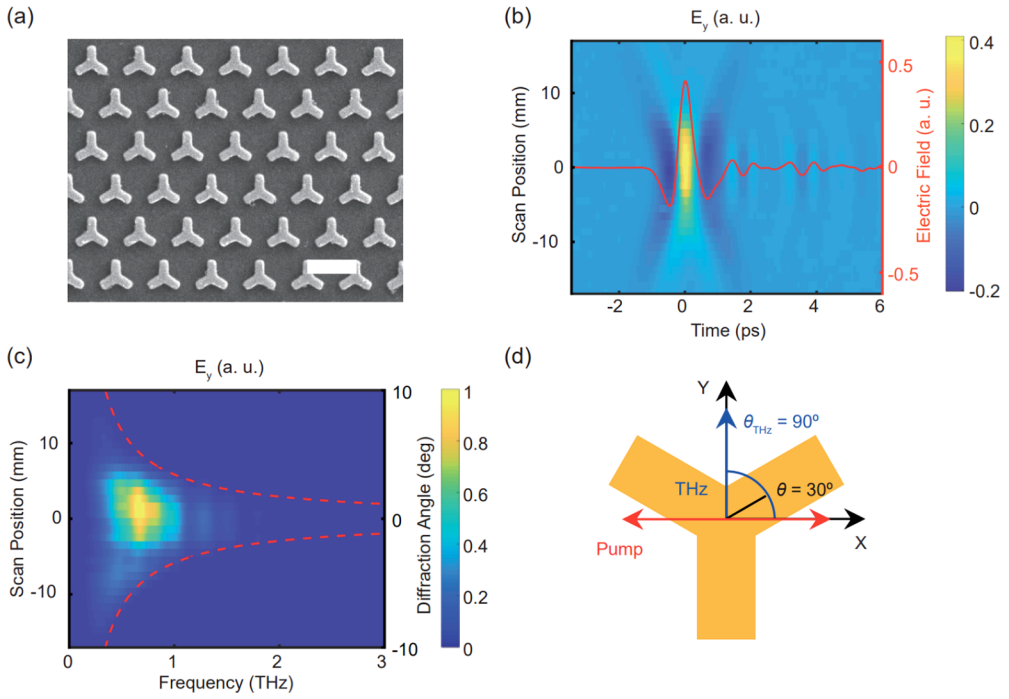

Figure 1. (a) Scanning electron microscope (SEM) image of the fabricated uniform C3 metasurface. Scale bar = 550 nm. (b) Generated THz electric field in the time domain with a 0.6 ps pulse duration and (c) the normalized absolute value of the electric field in the frequency domain. The measurable THz spectrum extends up to 2.5 THz. (d) Linear polarization of the generated THz wave is rotated by 3θ relative to the angle between the pump polarization and the meta-atom. This concept is illustrated for a linearly polarized beam along the *x*-axis with a relative meta-atom rotational displacement of 30°, which results in a subsequent rotation of the generated THz field by 90° to the *y*-axis.

realized, including second and third harmonic generation,[28−32] high harmonic generation,[33] quantum entanglement of photon states,[34] emission of single photons,[35] and THz wave generation.[36] Specifically, for nonlinear THz emission from plasmonic meta-atoms, laser intensity dependent generation mechanisms have been proposed, such as optical rectification,[37] acceleration of photoejected electrons by ponderomotive forces,[36] and subcycle bursts of tunneling currents.[38]

Moreover, the ability to spatially tailor the metasurface allows for the manipulation of both the near and far fields of the emitted light. This ability was used to demonstrate various types of nonlinear metasurfaces for beam steering,[39] beam shaping,[40] holography,[41] and imaging.[42] One of the most useful means to control the local phase and polarization of the interacting light in both linear and nonlinear metasurfaces relies on the concept of the Pancharatnam−Berry (P−B) phase.[43,44] This concept links the local orientation and symmetry of the individual meta-atom with the polarization and phase of the pump and generated photons.

Recently, functional THz emitters based on the principles of nonlinear P−B phase and optical rectification were demonstrated for the first time.[45] This concept was used to show control over the polarization of the emitted THz waves and generation of spatially separated left-hand and right-hand circularly polarized (LCP and RCP) THz waves as well as multicycle THz waves with polarization dispersion in time. While unveiling the potential of nonlinear P−B phase THz emitters, mechanisms that allow one to control the basic linear polarization states of THz waves at the diffraction order were not demonstrated to date. Here, we close this gap and demonstrate new mechanisms that allow one to obtain beam steering with continuous polarization control as well as full phase control of the generated THz photons. Two concepts are introduced, the first consists of a metagrating with a binary phase modulation and the second a metagrating with interlaced phase gradients. It is shown experimentally that both independent concepts allow continuous control of the linear polarization of THz waves in the emitted diffraction orders.

RESULTS AND DISCUSSION

THz Generation from Uniform C3 Meta-Atom Arrays.

First, to test the performance of our THz generation and measurement system, we used a control metasurface, which is similar to the one demonstrated in ref 45. The THz emitting metasurface was fabricated on a 15 nm thick ITO coated glass substrate. It consists of uniform hexagonal arrays of gold meta-atoms with C3 rotational symmetry and a lattice spacing of 550 nm, as shown in Figure 1a. The metasurfaces were fabricated using a three step lithography process (see Methods). The linear transmittance of the fabricated metasurface indicates the existence of a localized plasmon resonance between 1100 and 1600 nm (see Figure S1). From our previous work on second harmonic generation (SHG) on a gold-ITO hybrid metasurface, it was found that the SHG signals can be greatly enhanced when the pump wavelength is close to the epsilon-near-zero (ENZ) condition of the ITO film.[46] It is reasonable to assume that the ENZ effect can also contribute to enhanced THz emission in a gold-ITO hybrid device, as was very recently confirmed experimentally.[47] However, in this work, the ENZ effect is not our main focus. Alternatively, we chose the pump wavelength at 1500 nm, which is also located in the range of plasmonic resonance (see Figure S1) but far from the ENZ wavelength of ITO (~1160 nm). The metasurface was illuminated from the glass substrate side with linearly polarized ultrashort laser pulses (~50 fs pulse duration, 1500 nm central

https://doi.org/10.1021/acs.nanolett.1c04135
Nano Lett. XXXX, XXX, XXX−XXX

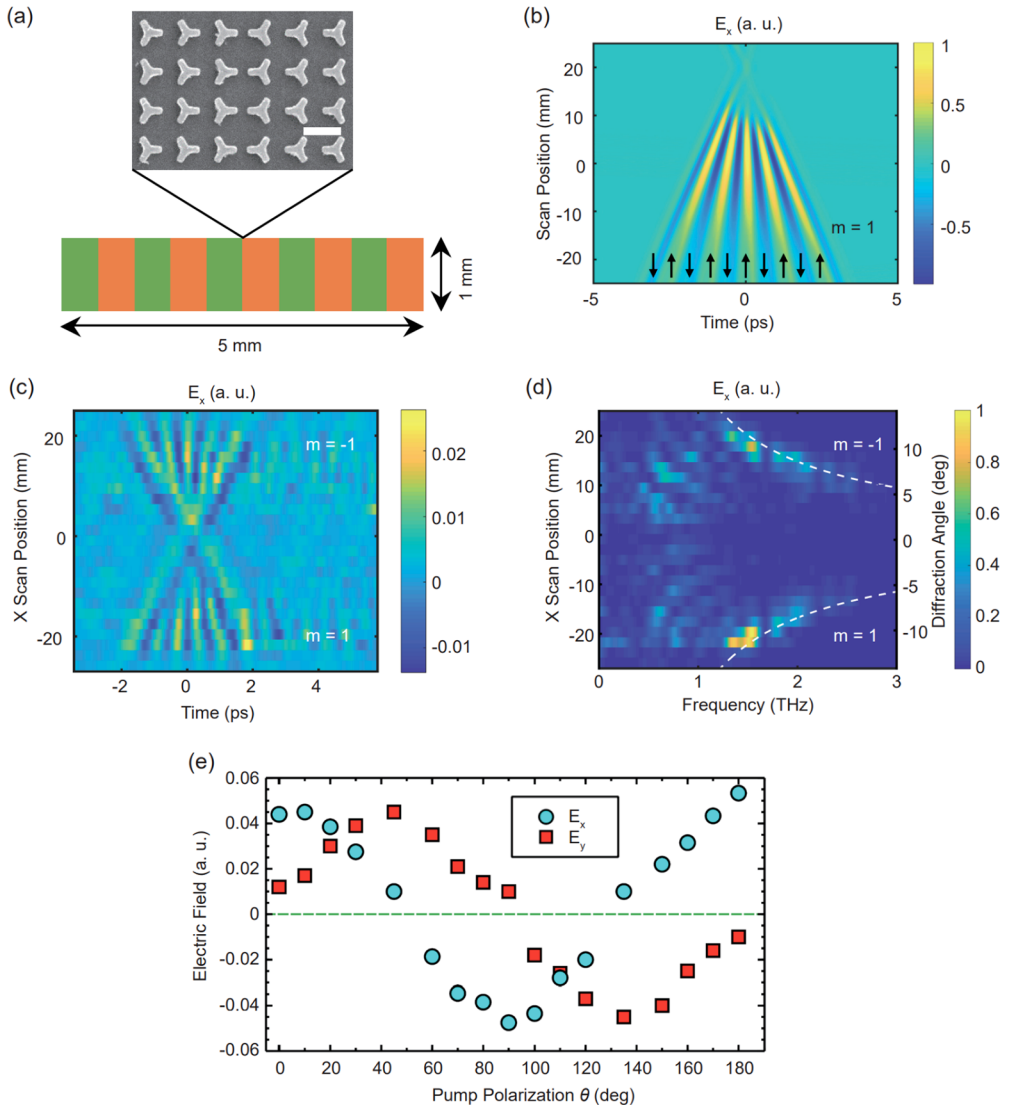

Figure 2. (a) SEM image and metagrating concept for the generation and control of THz waves using a binary phase modulation. The meta-atoms are arranged in a 1 mm unit-cell where the meta-atoms are inverted with a duty cycle of 0.5. Scale bar = 550 nm. (b) Beam propagation simulation for such a metagrating showing the THz E_x field in the $m = 1$ order. In each half cycle, the direction of the THz E_x component is reversed. (c) Measured THz E_x of the $m = \pm 1$ diffraction orders after illumination with a 1500 nm E_y pump wave. The THz fields have a 5-cycle temporal variation. (d) Frequency domain spatial profile of both THz diffraction orders, with collected frequencies ranging from approximately 1.0 THz to 2.5 THz. The collection bandwidth is limited by the NA of the off-axis parabolic mirror. (e) The rotation of the linearly polarized THz waves in the $m = +1$ diffraction order is examined by rotating the pump polarization and measuring the corresponding E_x and E_y components. The electric field modulation in the ZnTe nonlinear crystal indicates a complete tunable linear polarization direction of the THz waves.

wavelength, 100 μJ per pulse, beam size 1.5 mm × 6.0 mm), which leads to the emission of single cycle THz pulses in agreement with previous works.[37,45] The spatiotemporal properties of the generated THz pulses were measured using a time domain spectroscopy setup (Methods and Supporting Information section S2), whereby the generated ultrashort THz pulse is overlapped in a ZnTe nonlinear crystal with a synchronized time-delayed probe pulse. For the metagratings used in this study, the primary changes in the meta-atom orientations occur along the x spatial dimension, and as such the spatial properties are only raster scanned in this dimension, which allows all the necessary amplitude and polarization data to be measured. The THz time domain and frequency domain spatial profiles are shown in Figure 1b,c after collimation with a parabolic mirror (f = 101.6 mm). The generated THz pulses show a near one cycle profile with a pulse duration of approximately 0.6 ps, with a corresponding frequency spectrum centered at approximately 1.0 THz and extending out to ~2.5 THz. The upper frequency is limited by the detection range of the ZnTe crystal. The absolute conversion efficiency of a 30 nm thick plasmonic metasurface is estimated to be 6×10^{-8}. This conversion efficiency is comparable to that of ~550 times thick ZnTe crystal excited under the same experimental conditions (Figure S3).[47] In addition, based on the concept of the nonlinear P−B phase with respect to the C3 meta-atom, the linear polarization of the emitted THz waves can be continuously rotated through rotating the linear polarization direction of the pump wave. When the linear polarization of the pump wave is at an angle θ with respect to the principal axis of the meta-atom, the linear polarization of the THz wave is rotated by 3θ, which was verified in ref 45 and is illustrated in Figure 1d.

https://doi.org/10.1021/acs.nanolett.1c04135
Nano Lett. XXXX, XXX, XXX−XXX

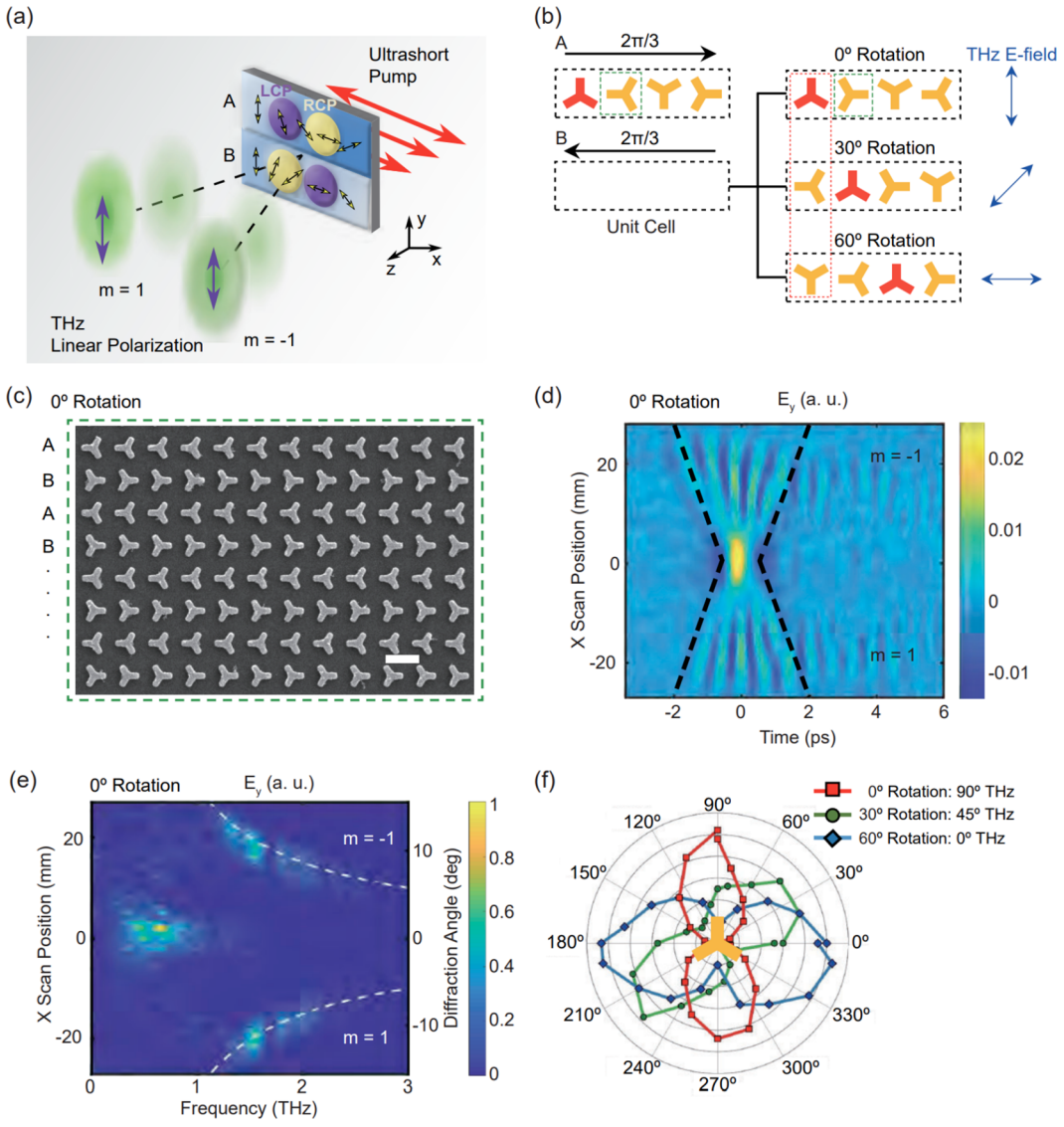

Figure 3. (a) Generation of linearly polarized THz waves in the far field using metagratings with interlaced phase gradients. The metagrating consists of consecutive phase gradient rows which rotate in opposite directions across the metasurface. The consecutive phase gradient metagratings emit THz waves with LCP and RCP components to opposite diffraction orders, leading to an overlap of the LCP and RCP components, and thus a linear polarization state of the THz waves can be obtained in the far field diffraction orders. (b) Schematic showing the lateral phase shift between the meta-atoms in the consecutive rows A and B. Three metagrating devices with the relative rotation angle of 0°, 30°, and 60° in row B were chosen to demonstrate the proposed concept. (c) SEM image of a section of the fabricated 0° phase shift metasurface. Scale bar: 550 nm. The green box indicates the area of meta-atoms shown in the corresponding green boxes in part b. (d) Linearly polarized E_y fields in the $m = \pm 1$ diffraction orders. The black dashed lines are a guide to the THz wavepacket region. (e) Frequency spectra of the ± 1 diffraction orders, with frequencies ranging from 1.0 to 2.5 THz. The white dashed lines indicate the expected Raman−Nath diffraction angles. (f) Measured electric field direction as a function of the rotation angle of a THz wire grid polarizer. The linear polarized electric fields of the THz waves are along y, 45°, and x directions for the 0°, 30°, and 60° rotation metagrating, respectively.

THz Metagratings with Binary Phase. Next, a 5.0 mm × 1.0 mm binary phase metagrating was fabricated with a lattice constant of $\Lambda = 1.0$ mm. The metagrating lattice constant and dimensions were chosen in order to collect the maximum generated electric fields of the $m = \pm 1$ diffraction orders into the numerical aperture (NA) of the system (see Figure S2). In each half period of the grating, a π binary phase shift is applied to the meta-atoms, as shown in Figure 2a. The simulated spatiotemporal E_x electric field profile of the $m = +1$ order of such a metagrating is shown in Figure 2b (see Methods for simulation details). The resulting electric field consists of five complete cycles in time and each consists of two half cycles where the E_x electric field undergoes a π phase shift per half cycle. The five temporal cycles originate from space to time mapping between the metasurface and the generated THz pulse.[48] The experimental spatiotemporal E_x field profile emitted from the metagrating after ultrashort pulse illumination is shown in Figure 2c. The top and bottom parts of the spatial scan capture the generated electric field in the $m = \pm 1$ diffraction orders. Multicycle electric fields are measured in each diffraction order, with an overall reversed electric field phase between the two diffraction orders. Figure 2d shows the corresponding spatio-spectral map of the generated THz field, consisting of spatially dispersed frequencies from approximately 1.0 to 2.5 THz. Frequencies below 1.0 THz are generated; however, they are diffracted outside the NA of the

https://doi.org/10.1021/acs.nanolett.1c04135
Nano Lett. XXXX, XXX, XXX−XXX

collection system. The frequency dependent diffraction follows the expected angles according to the Raman−Nath condition: $\sin\theta_m(\lambda_{THz}) = m\lambda_{THz}/\Lambda + \sin\theta_{in}$, where m is the diffraction order, λ_{THz} is the wavelength of the generated THz wave, and θ_{in} is the incident angle of the pump wave.[49] In the frequency domain across the spatial position, a number of periodic features can be noted between 0.8−1.0 THz. This is due to the convolution of the generated frequencies with a *sinc* function, which is related to the binary modulation and the finite size of the metagrating.[49] The total diffraction efficiency for the binary phase grating was estimated from the measurements to be ≈65%, which was calculated as the fraction of the THz fields diffracted into the predicted Raman−Nath ±1 diffraction orders and the fraction of the field diffracted as a sinc amplitude modulation across the spatial profile. This estimation does not take into account the THz field diffracted into higher orders (such as third and fifth), which are outside the collection NA of the optical system. The angle of diffraction and the number of temporal cycles are directly related to the overall metasurface length and number of lattice periods.[49]

Increased functionality of the metagrating is achieved through the ability to continuously tune the linear polarization direction of the THz at the generated diffraction orders, by rotating the linear polarization angle of the pump waves. This is due to the fixed 3θ phase relationship between the pump and the generated THz fields.[45] This functionality of the metagrating is specifically important since the all-optical polarization control is very simple and reduces the need for lossy and bulky THz elements. Furthermore, modulation of the THz polarization direction could potentially be achieved at fast switching rates through the use of a Pockels cell on the pump beam. The all-optical tuning of the polarization of THz wave in the diffraction directions was measured and is shown in Figure 2e. The measured E_y and E_x, for a cross-section of the $m = +1$ order, are shown for a range of 0−180° rotation of the linear polarization direction of the pump wave. The resulting THz field maxima of the E_x component occurs at $\theta_{Pump} = 0°$, $\Delta\theta_{THz} = 0°$ (E_x) and $\theta_{Pump} = 90°$, $\Delta\theta_{THz} = 270°$ (E_x). The corresponding E_y maxima occur at pump polarization angles of $\theta_{Pump} = 45°$ and 135°. The continuous transition between the maxima locations indicates the continuous rotation of the linearly polarized THz waves. Due to the periodic modulation of the meta-atoms, the linear THz polarization angle of the −1 and +1 orders rotate in opposite directions.

THz Metagratings with Interlaced Phase Gradients. Periodic binary phase distributions of the C3 meta-atoms provide the simplest method to develop THz metagratings; however, in such a configuration, the generated THz waves at the diffraction orders always have an opposite overall electric field phase. Also, the binary phase modulation leads to THz emission into multiple higher diffraction orders which reduce the efficiency of emission into the intended diffraction orders.[49] Another way to realize a THz metagrating is to introduce interlaced continuous phase gradients. This can be done by spatially rotating the C3 meta-atoms through 120° over each grating period. This local linear polarization gradient results in a continuous phase gradient and emission of two THz waves in opposite spatial directions to the ±1 orders, with RCP and LCP polarization state, respectively. A full discussion on the C3 meta-atom selection rules and general THz emission characteristics of phase gradient THz emitters can be found in our previous work.[45] Here, we examine the effect of subwavelength interlacing of metagratings with opposite phase gradient and show that it leads to a microscopic interference of the THz waves. As shown in Figure 3a, this interference can be used to obtain metagrating emitters with linear polarization states controlled by design as well as all-optically.

In this approach, the imparted phase gradients of the C3 meta-atoms are arranged in two consecutive repeating rows, where the phase gradients are reversed in each row, here labeled A and B. In Figure 3b, we designed three metagrating devices, where the first C3 meta-atom in row B has a relative rotation angle of $\theta = 0°$, 30°, 60° with respect to the one in row A, respectively. A relative spatial shift (represented by the C3 meta-atom with red color) in row B is introduced. In this case, the THz wave from the first C3 meta-atom in row B (denoted by the red color dashed line) has a nonlinear P−B phase of 3θ. An SEM image of the 0° rotation metagrating is shown in Figure 3c. The THz emission in row A with LCP and RCP polarization states goes to the ±1 diffraction orders. In comparison, the THz waves with LCP and RCP states from the row B go to the opposite −1 and +1 orders. The superimposed THz waves of two in phase LCP and RCP polarization states leads to a linearly polarized electric field pointing along the y axis. The polarization direction of the linearly polarized THz wave can be rotated through imparting a phase shift between the meta-atoms in the corresponding A and B rows. A $\theta = 30°$ rotation of the first meta-atom in row B will result in a $3\theta = 90°$ phase shift between the LCP and RCP states, and thus the linearly polarized THz wave is rotated by an angle of $3\theta/2$, i.e., 45° direction. Furthermore, a $\theta = 60°$ rotation of the first meta-atom in the B row will likewise further rotate the linearly polarized THz wave by 90°, i.e., to the x axis.

In order to experimentally verify this idea, three 5.0 mm × 1.0 mm metagratings were fabricated with meta-atom relative rotation angles of 0°, 30°, and 60° in row B (Figure 3b). The consecutive phase gradients were rotated through 120°/mm, resulting in 5 periods across 5.0 mm. Each metasurface was illuminated with linearly polarized pump waves orientated along the x-direction. Figure 3d shows the measured spatiotemporal THz diffraction pattern for the 0° rotation metagrating. The generated THz fields in the ±1 diffraction orders, consisting of two 5-cycle temporal profiles, are y-polarized and overall in phase. The corresponding spatial frequency spectrum is shown in Figure 3e, with frequencies between 1.0 THz and 2.5 THz. The vast majority of the generated THz waves in the collected aperture are diffracted into the $m = \pm1$ orders (∼90%); however, a small low-frequency portion is visible in the center of the scanning region. This diffraction efficiency is significantly higher than that of the binary phase gratings shown in Figure 2. Illuminating the 0° and 30° rotation metagratings results in linearly polarized fields at the $\hat{x}$ and $\frac{1}{\sqrt{2}}(\hat{x} + \hat{y})$ directions, respectively (see Figure S5). In order to confirm the exact linear polarization direction of the diffracted THz waves, the transmission of the electric field through a THz polarizer was examined. As shown in Figure 3f, the electric field shows peak values at the polarizer transmission angles predicted by our theory. The picture of interference of circular polarization states relates directly to the notion of Pancharatnam−Berry phase on THz phase gradient metasurface.[45]

https://doi.org/10.1021/acs.nanolett.1c04135
Nano Lett. XXXX, XXX, XXX−XXX

To conclude, in this study we show the application of THz metagrating emitters to enable the generation of broadband linearly polarized THz waves. First, the concept of a conventional periodic poling technique was utilized to design a metagrating with a binary phase. The broadband THz waves in the diffraction orders are generated, and their linear polarization directions can be simply controlled through the rotation of the polarization direction of the pumping wave. In a more complex manner, we show that the far field polarization state can also be tuned through the interference of THz waves from interlaced metasurfaces. The operation of the THz metagratings with reversed phase gradients are demonstrated through the nonlinear P−B phase notion, which results in a higher diffraction efficiency relative to binary phase methods. As such, the proposed metagrating strategies can be used for complete control of the linear polarization state, relative phase in the two diffraction orders, diffraction angle, and number of temporal field cycles of the generated THz waves. These unique functionalities of THz metagratings allow for a direct and customizable control of THz waves, which is highly attractive for THz applications.

METHODS

Fabrication of the Metagratings. The metagratings used in this study were fabricated using an electron beam lithography (EBL) process. First, a thin positive electron resist layer (PMMA, ALLRESIST) was prepared on a ITO (∼15 nm thick) coated glass substrate using spin-coating. This was followed by baking the resist at 180 °C for 3 min. The designed phase patterns of the metasurfaces were transferred to the resist layer using a EBL process. Afterward, a 30 nm thick gold film was deposited onto the resist using the electron beam evaporation method. This finally forms the gold plasmonic metagratings after a lift-off process.

THz Time Domain Spectroscopy. Time domain spectroscopy (TDS) was used to measure the spatiotemporal profile of the THz waves emitted from the fabricated metasurfaces and metagratings. The laser used is a femtosecond laser source (Spectra-Physics Solstice Ace) that generates pulses at a wavelength of 800 nm, with a 2.0 kHz repetition rate, 3.5 mJ per pulse, and with a pulse duration of ∼35 fs. The output is spilt into the pump and the probe lines. On the pump line 3 mJ of the laser power is taken and directed into an optical parametric amplifier (TOPAS) where ultrashort pulses with wavelengths from 450 nm to 2800 nm can be generated. All experiments were performed with 1500 nm as the wavelength of choice. The metasurface is placed at the focal point of an off-axis parabolic mirror (f = 101.6 mm) which collects and collimates the generated THz light. Before the parabolic mirror, a 5 mm Teflon slab is used to filter the pump beam. In the collimated plane a motorized stage and slit can be used to sample the spatial features of the THz beam profile. A second off-axis parabolic mirror (f = 101.6 mm) focuses the generated THz into a nonlinear ZnTe electro-optic crystal. On the probe line, a small portion of the 800 nm ultrashort pulses are sent to a motorized delay stage which is used to control the temporal overlap between the probe and THz pulses in the ZnTe crystal. The probe pulse is then directed through a 3 mm hole in the second parabolic mirror and is incident on the ZnTe crystal. After passing through the ZnTe nonlinear crystal, the THz electro-optic effect on the probe was measured by an optical set composed of a quarter wave plate, a Wollaston prism, and a balanced photodiode.

THz Propagation Simulations. The simulations were based on the beam propagation technique and performed using MATLAB. The broadband pulse was defined by a spectrum matching the measured THz signal. According to the rotational orientation of the meta-atoms, the spectral amplitudes and signs of the electric field components are defined for each frequency on the metasurface plane and set to zero outside the metasurface. The spatial Fourier components of the field $E(k_x)$ propagates along the propagation direction, z, for each temporal frequency, f, by phase addition of $k_z z$. The collimation of the beam by a parabolic mirror was simulated by phase addition. The propagated spatio-spectral structure was then used to reconstruct the spatiotemporal field by inverse Fourier transform in the time and space domains.

ASSOCIATED CONTENT

Supporting Information

The Supporting Information is available free of charge at https://pubs.acs.org/doi/10.1021/acs.nanolett.1c04135.

Linear optical properties of the metasurfaces, THz time domain spectroscopy, absolute efficiency of THz emission, metagrating with binary phase and THz diffraction, and interlacing metagratings and time domain profile of THz waves (PDF)

AUTHOR INFORMATION

Corresponding Authors

Tal Ellenbogen − *Department of Physical Electronics, School of Electrical Engineering, Tel-Aviv University, 6997801 Tel Aviv, Israel; Center for Light-Matter Interaction, Tel-Aviv University, 6779801 Tel-Aviv, Israel*; Email: tellenbogen@tauex.tau.ac.il

Guixin Li − *Shenzhen Institute for Quantum Science and Engineering and Department of Materials Science and Engineering, Southern University of Science and Technology, 518055 Shenzhen, China*; orcid.org/0000-0001-9689-8705; Email: ligx@sustech.edu.cn

Authors

Cormac McDonnell − *Department of Physical Electronics, School of Electrical Engineering, Tel-Aviv University, 6997801 Tel Aviv, Israel; Center for Light-Matter Interaction, Tel-Aviv University, 6779801 Tel-Aviv, Israel*; orcid.org/0000-0003-1251-9339

Junhong Deng − *Shenzhen Institute for Quantum Science and Engineering and Department of Materials Science and Engineering, Southern University of Science and Technology, 518055 Shenzhen, China*

Symeon Sideris − *Department of Physical Electronics, School of Electrical Engineering, Tel-Aviv University, 6997801 Tel Aviv, Israel; Center for Light-Matter Interaction, Tel-Aviv University, 6779801 Tel-Aviv, Israel*

Complete contact information is available at: https://pubs.acs.org/10.1021/acs.nanolett.1c04135

Author Contributions

[+]C.M. and J.D. contributed equally to this work. G.L. and T.E. conceived the ideas and supervised the project, C.M. conducted the THz measurements, J.D. fabricated the metasurfaces, and S.S. conducted the electromagnetic simulations. C.M., T.E., and G.L. wrote the manuscript. All authors participated in the discussions.

https://doi.org/10.1021/acs.nanolett.1c04135
Nano Lett. XXXX, XXX, XXX−XXX

Notes

The authors declare no competing financial interest.

■ ACKNOWLEDGMENTS

G.L. is financially supported by National Natural Science Foundation of China (Grants 91950114 and 11774145), Guangdong Provincial Innovation and Entrepreneurship Project (Grant 2017ZT07C071), and Natural Science Foundation of Shenzhen Innovation Commission (Grant JCYJ20200109140808088). T.E. declares that this publication is part of a project that has received funding from the European Research Council (ERC) under the European Union's Horizon 2020 research and innovation program (Grant Agreement No. 715362). G.L. and T.E. would like to thank the support from NSFC-ISF joint grant (Grant 12161141010; 3450/21). The authors would like to thank Ido Nagler for the design and fabrication of the sample holders.

■ REFERENCES

(1) Yang, X.; Zhao, X.; Yang, K.; Liu, Y.; Liu, Y.; Fu, W.; Luo, Y. Biomedical Applications of Terahertz Spectroscopy and Imaging. *Trends Biotechnol.* **2016**, *34*, 810−824.

(2) Smolyanskaya, O. A.; Chernomyrdin, N. V.; Konovko, A. A.; Zaytsev, K. I.; Ozheredov, I. A.; Cherkasova, O. P.; Nazarov, M. M.; Guillet, J.-P.; Kozlov, S. A.; Kistenev, Y. V.; Coutaz, J.-L.; Mounaix, P.; Vaks, V. L.; Son, J.-H.; Cheon, H.; Wallace, V. P.; Feldman, Y.; Popov, I.; Yaroslavsky, A. N.; Shkurinov, A. P.; Tuchin, V. V. Terahertz Biophotonics as a Tool for Studies of Dielectric and Spectral Properties of Biological Tissues and Liquids. *Prog. Quantum Electron.* **2018**, *62*, 1−77.

(3) Kanda, N.; Konishi, K.; Nemoto, N.; Midorikawa, K.; Kuwata-Gonokami, M. Real-Time Broadband Terahertz Spectroscopic Imaging by Using a High-Sensitivity Terahertz Camera. *Sci. Rep.* **2017**, *7*, 42540.

(4) Jin, K. H.; Kim, Y.-G.; Cho, S. H.; Ye, J. C.; Yee, D.-S. High-Speed Terahertz Reflection Three-Dimensional Imaging for Non-destructive Evaluation. *Opt. Express* **2012**, *20*, 25432−25440.

(5) Gowen, A. A.; O'Sullivan, C.; O'Donnell, C. P. Terahertz Time Domain Spectroscopy and Imaging: Emerging Techniques for Food Process Monitoring and Quality Control. *Trends Food Sci. Technol.* **2012**, *25*, 40−46.

(6) Federici, J. F.; Schulkin, B.; Huang, F.; Gary, D.; Barat, R.; Oliveira, F.; Zimdars, D. THz Imaging and Sensing for Security Applications—Explosives, Weapons and Drugs. *Semicond. Sci. Technol.* **2005**, *20*, S266−S280.

(7) Lu, M.; Shen, J.; Li, N.; Zhang, Y.; Zhang, C.; Liang, L.; Xu, X. Detection and Identification of Illicit Drugs Using Terahertz Imaging. *J. Appl. Phys.* **2006**, *100*, 103104.

(8) Ducournau, G.; Szriftgiser, P.; Pavanello, F.; Peytavit, E.; Zaknoune, M.; Bacquet, D.; Beck, A.; Akalin, T.; Lampin, J.-F.; Lampin, J.-F. THz Communications Using Photonics and Electronic Devices: The Race to Data-Rate. *J. Infrared, Millimeter, Terahertz Waves* **2015**, *36*, 198−220.

(9) Nagatsuma, T.; Ducournau, G.; Renaud, C. C. Advances in Terahertz Communications Accelerated by Photonics. *Nat. Photonics* **2016**, *10*, 371−379.

(10) Odaka, D.; Ohki, Y. Terahertz Spectroscopic Analysis of Crystal Growth in Poly(Ethylene Naphthalate). *Jpn. J. Appl. Phys.* **2017**, *56*, 072401.

(11) Valdés Aguilar, R.; Qi, J.; Brahlek, M.; Bansal, N.; Azad, A.; Bowlan, J.; Oh, S.; Taylor, A. J.; Prasankumar, R. P.; Yarotski, D. A. Time-Resolved Terahertz Dynamics in Thin Films of the Topological Insulator Bi_2Se_3. *Appl. Phys. Lett.* **2015**, *106*, 011901.

(12) Fleischer, S.; Zhou, Y.; Field, R. W.; Nelson, K. A. Molecular Orientation and Alignment by Intense Single-Cycle THz Pulses. *Phys. Rev. Lett.* **2011**, *107*, 163603.

(13) Kampfrath, T.; Sell, A.; Klatt, G.; Pashkin, A.; Mährlein, S.; Dekorsy, T.; Wolf, M.; Fiebig, M.; Leitenstorfer, A.; Huber, R. Coherent Terahertz Control of Antiferromagnetic Spin Waves. *Nat. Photonics* **2011**, *5*, 31−34.

(14) Chen, J.; Chai, L.; Song, Q.; Hu, M. Metal Particles Filled Gratings with High Diffraction Efficiency for Terahertz Wave by Traditional Mask Production. *Infrared Phys. Technol.* **2020**, *111*, 103511.

(15) Squires, A. D.; Constable, E.; Lewis, R. A. 3D Printed Terahertz Diffraction Gratings And Lenses. *J. Infrared, Millimeter, Terahertz Waves* **2015**, *36*, 72−80.

(16) Scherger, B.; Born, N.; Jansen, C.; Schumann, S.; Koch, M.; Wiesauer, K. Compression Molded Terahertz Transmission Blaze-Grating. *IEEE Trans. Terahertz Sci. Technol.* **2012**, *2*, 556−561.

(17) Monnai, Y.; Altmann, K.; Jansen, C.; Hillmer, H.; Koch, M.; Shinoda, H. Terahertz Beam Steering and Variable Focusing Using Programmable Diffraction Gratings. *Opt. Express* **2013**, *21*, 2347−2354.

(18) Yamada, I.; Takano, K.; Hangyo, M.; Saito, M.; Watanabe, W. Terahertz Wire-Grid Polarizers with Micrometer-Pitch Al Gratings. *Opt. Lett.* **2009**, *34*, 274−276.

(19) Zhang, B.; Gong, Y. Achromatic Terahertz Quarter Waveplate Based on Silicon Grating. *Opt. Express* **2015**, *23*, 14897−14902.

(20) Khusyainov, D.; Ovcharenko, S.; Gaponov, M.; Buryakov, A.; Klimov, A.; Tiercelin, N.; Pernod, P.; Nozdrin, V.; Mishina, E.; Sigov, A.; Preobrazhensky, V. Polarization Control of THz Emission Using Spin-Reorientation Transition in Spintronic Heterostructure. *Sci. Rep.* **2021**, *11*, 697.

(21) Hibberd, M. T.; Lake, D. S.; Johansson, N. A. B.; Thomson, T.; Jamison, S. P.; Graham, D. M. Magnetic-Field Tailoring of the Terahertz Polarization Emitted from a Spintronic Source. *Appl. Phys. Lett.* **2019**, *114*, 031101.

(22) Niwa, H.; Yoshikawa, N.; Kawaguchi, M.; Hayashi, M.; Shimano, R. Switchable Generation of Azimuthally- and Radially-Polarized Terahertz Beams from a Spintronic Terahertz Emitter. *Opt. Express* **2021**, *29*, 13331−13343.

(23) Choi, W. J.; Cheng, G.; Huang, Z.; Zhang, S.; Norris, T. B.; Kotov, N. A. Terahertz Circular Dichroism Spectroscopy of Biomaterials Enabled by Kirigami Polarization Modulators. *Nat. Mater.* **2019**, *18*, 820−826.

(24) Gueckstock, O.; Nádvorník, L.; Seifert, T. S.; Borchert, M.; Jakob, G.; Schmidt, G.; Woltersdorf, G.; Kläui, M.; Wolf, M.; Kampfrath, T. Modulating the Polarization of Broadband Terahertz Pulses from a Spintronic Emitter at Rates up to 10 kHz. *Optica* **2021**, *8*, 1013−1019.

(25) George, D. K.; Stier, A. V.; Ellis, C. T.; McCombe, B. D.; Černe, J.; Markelz, A. G. Terahertz Magneto-Optical Polarization Modulation Spectroscopy. *J. Opt. Soc. Am. B* **2012**, *29*, 1406−1412.

(26) Yatsugi, K.; Matsumoto, N.; Nagashima, T.; Hangyo, M. Transport Properties of Free Carriers in Semiconductors Studied by Terahertz Time-Domain Magneto-Optical Ellipsometry. *Appl. Phys. Lett.* **2011**, *98*, 212108.

(27) O'Sullivan, C. M.; Murphy, J. A. *Field Guide to Terahertz Sources, Detectors, and Optics*; SPIE, 2012.

(28) Klein, M. W.; Enkrich, C.; Wegener, M.; Linden, S. Second-Harmonic Generation from Magnetic Metamaterials. *Science.* **2006**, *313*, 502−504.

(29) Husu, H.; Siikanen, R.; Mäkitalo, J.; Lehtolahti, J.; Laukkanen, J.; Kuittinen, M.; Kauranen, M. Metamaterials with Tailored Nonlinear Optical Response. *Nano Lett.* **2012**, *12*, 673−677.

(30) Salomon, A.; Zielinski, M.; Kolkowski, R.; Zyss, J.; Prior, Y. Size and Shape Resonances in Second Harmonic Generation from Silver Nanocavities. *J. Phys. Chem. C* **2013**, *117*, 22377−22382.

(31) Kruk, S.; Weismann, M.; Bykov, A. Y.; Mamonov, E. A.; Kolmychek, I. A.; Murzina, T.; Panoiu, N. C.; Neshev, D. N.; Kivshar, Y. S. Enhanced Magnetic Second-Harmonic Generation from Resonant Metasurfaces. *ACS Photonics* **2015**, *2*, 1007−1012.

(32) Chen, S.; Zeuner, F.; Weismann, M.; Reineke, B.; Li, G.; Valev, V. K.; Cheah, K. W.; Panoiu, N. C.; Zentgraf, T.; Zhang, S. Giant

https://doi.org/10.1021/acs.nanolett.1c04135
Nano Lett. XXXX, XXX, XXX−XXX

Nonlinear Optical Activity of Achiral Origin in Planar Metasurfaces with Quadratic and Cubic Nonlinearities. *Adv. Mater.* **2016**, *28*, 2992−2999.
(33) Liu, H.; Guo, C.; Vampa, G.; Zhang, J. L.; Sarmiento, T.; Xiao, M.; Bucksbaum, P. H.; Vučković, J.; Fan, S.; Reis, D. A. Enhanced High-Harmonic Generation from an All-Dielectric Metasurface. *Nat. Phys.* **2018**, *14*, 1006−1010.
(34) Marino, G.; Solntsev, A. S.; Xu, L.; Gili, V. F.; Carletti, L.; Poddubny, A. N.; Rahmani, M.; Smirnova, D. A.; Chen, H.; Lemaître, A.; Zhang, G.; Zayats, A. V.; De Angelis, C.; Leo, G.; Sukhorukov, A. A.; Neshev, D. N. Spontaneous Photon-Pair Generation from a Dielectric Nanoantenna. *Optica* **2019**, *6*, 1416−1422.
(35) Kan, Y.; Andersen, S. K. H.; Ding, F.; Kumar, S.; Zhao, C.; Bozhevolnyi, S. I. Metasurface-Enabled Generation of Circularly Polarized Single Photons. *Adv. Mater.* **2020**, *32*, 1907832.
(36) Polyushkin, D. K.; Hendry, E.; Stone, E. K.; Barnes, W. L. THz Generation from Plasmonic Nanoparticle Arrays. *Nano Lett.* **2011**, *11*, 4718−4724.
(37) Luo, L.; Chatzakis, I.; Wang, J.; Niesler, F. B. P.; Wegener, M.; Koschny, T.; Soukoulis, C. M. Broadband Terahertz Generation from Metamaterials. *Nat. Commun.* **2014**, *5*, 3055.
(38) Takano, K.; Asai, M.; Kato, K.; Komiyama, H.; Yamaguchi, A.; Iyoda, T.; Tadokoro, Y.; Nakajima, M.; Bakunov, M. I. Terahertz Emission from Gold Nanorods Irradiated by Ultrashort Laser Pulses of Different Wavelengths. *Sci. Rep.* **2019**, *9*, 3280.
(39) Keren-Zur, S.; Avayu, O.; Michaeli, L.; Ellenbogen, T. Nonlinear Beam Shaping with Plasmonic Metasurfaces. *ACS Photonics* **2016**, *3*, 117−123.
(40) Li, G.; Wu, L.; Li, K. F.; Chen, S.; Schlickriede, C.; Xu, Z.; Huang, S.; Li, W.; Liu, Y.; Pun, E. Y. B.; Zentgraf, T.; Cheah, K. W.; Luo, Y.; Zhang, S. Nonlinear Metasurface for Simultaneous Control of Spin and Orbital Angular Momentum in Second Harmonic Generation. *Nano Lett.* **2017**, *17*, 7974−7979.
(41) Zheng, G.; Mühlenbernd, H.; Kenney, M.; Li, G.; Zentgraf, T.; Zhang, S. Metasurface Holograms Reaching 80% Efficiency. *Nat. Nanotechnol.* **2015**, *10*, 308−312.
(42) Schlickriede, C.; Waterman, N.; Reineke, B.; Georgi, P.; Li, G.; Zhang, S.; Zentgraf, T. Imaging through Nonlinear Metalens Using Second Harmonic Generation. *Adv. Mater.* **2018**, *30*, 1703843.
(43) Jia, M.; Wang, Z.; Li, H.; Wang, X.; Luo, W.; Sun, S.; Zhang, Y.; He, Q.; Zhou, L. Efficient Manipulations of Circularly Polarized Terahertz Waves with Transmissive Metasurfaces. *Light Sci. Appl.* **2019**, *8*, 16.
(44) Li, G.; Chen, S.; Pholchai, N.; Reineke, B.; Wong, P. W. H.; Pun, E. Y. B.; Cheah, K. W.; Zentgraf, T.; Zhang, S. Continuous Control of the Nonlinearity Phase for Harmonic Generations. *Nat. Mater.* **2015**, *14*, 607−612.
(45) McDonnell, C.; Deng, J.; Sideris, S.; Ellenbogen, T.; Li, G. Functional THz Emitters Based on Pancharatnam-Berry Phase Nonlinear Metasurfaces. *Nat. Commun.* **2021**, *12*, 30.
(46) Deng, J.; Tang, Y.; Chen, S.; Li, K.; Zayats, A. V.; Li, G. Giant Enhancement of Second-Order Nonlinearity of Epsilon-near-Zero Medium by a Plasmonic Metasurface. *Nano Lett.* **2020**, *20*, 5421−5427.
(47) Lu, Y.; Feng, X.; Wang, Q.; Zhang, X.; Fang, M.; Sha, W. E. I.; Huang, Z.; Xu, Q.; Niu, L.; Chen, X.; Ouyang, C.; Yang, Y.; Zhang, X.; Plum, E.; Zhang, S.; Han, J.; Zhang, W. Integrated Terahertz Generator-Manipulators Using Epsilon-near-Zero-Hybrid Nonlinear Metasurfaces. *Nano Lett.* **2021**, *21*, 7699−7707.
(48) Blanchard, F.; Razzari, L.; Bandulet, H. C.; Sharma, G.; Morandotti, R.; Kieffer, J. C.; Ozaki, T.; Reid, M.; Tiedje, H. F.; Haugen, H. K.; Hegmann, F. A. Generation of 1.5 μJ Single-Cycle Terahertz Pulses by Optical Rectification from a Large Aperture ZnTe Crystal. *Opt. Express* **2007**, *15*, 13212−13220.
(49) Keren-Zur, S.; Ellenbogen, T. Direct Space to Time Terahertz Pulse Shaping with Nonlinear Metasurfaces. *Opt. Express* **2019**, *27*, 20837−20847.

https://doi.org/10.1021/acs.nanolett.1c04135
Nano Lett. XXXX, XXX, XXX−XXX